Contributed paper

OPTO-ELECTRONICS REVIEW **12**(1), 149–155 (2004)

Photodiode with resonant cavity based on InGaAs/InP for 1.9 μm band

J. ZYNEK*[1], A. JASIK[1], W. STRUPIŃSKI[1], J. RUTKOWSKI[2], A. JAGODA[1], K. PRZYBOROWSKA[1], R. JAKIEŁA[1], M. PIERSA[1], and A. WNUK[1]

[1]Institute of Electronic Materials Technology, 133 Wólczyńska Str., 01-919 Warsaw, Poland
[2]Institute of Applied Physics, Military University of Technology, 2 Kaliskiego Str., 00-908 Warsaw, Poland

The results of the work aiming at development of a RCE photodiode operating at 1.9 μm are described. Detection is based on interband absorption in a thin pseudomorphic InGaAs layer placed inside a resonant cavity which enhances an optical field. The technology of heterostructures grown by MOCVD has been developed. The photodiode structure comprises, between two parallel Bragg mirrors, an InP p-i-n junction with a thin strained $In_xGa_{1-x}As$ ($0.65 \le x \le 0.8$) layer placed inside an undoped region. The bottom Bragg mirror is composed of an $In_{0.53}Ga_{0.47}As/InP$ quarter-wave layer stack, the top mirror is made of Si/SiO_2 layers deposited on epitaxial layers by a sputtering method. Good properties of $In_xGa_{1-x}As$ strained layers and good reflectivity spectra of the Bragg mirrors enable us to obtain RCE photodetectors with photoresponse characteristics at wavelengths near 1.9 μm. Photodetectors exhibit very low dark current densities (of the order of 10^{-6} A/cm^2).

Keywords: RCE photodetector, InGaAs photodiode.

1. Introduction

Detection of a low level near infrared radiation at the wavelengths longer than 1.65 μm still remains a problem in spite of numerous studies on photodetectors for this spectral range and an increasing demand for these devices for many applications. This state results from the lack of good quality semiconductors with a suitable bandgap. The most mature is the technology of p-i-n photodiodes based on thick, strain-relaxed $In_xGa_{1-x}As$ ($0.6 < x \le 0.83$) epitaxial layers grown on the InP substrate. It enables us to tailor the cutoff wavelength by varying the alloy composition and to achieve a high sensivity to the wavelengths as long as 2.5 μm, but it does not allow the dark current densities at the room temperature to decrease below 10^{-3} A/cm^2 (at $U = -1$ V) [1,2]. This is caused by the difference in the lattice constants of both materials. Although the active layer of the thickness sufficient to absorb most of the detected radiation (≥ 2 μm) is grown on a stack of $InAs_yP_{1-y}$ buffer layers with abruptly increased lattice constants, it is not possible to avoid a very high density of misfit dislocations which become centres of the thermal generation of carriers. The high dark current density limits the photodiode detectivity to about 4×10^{10} cmHz$^{1/2}$/W at room temperature.

Reduction of the $In_xGa_{1-x}As$ layer thickness below the critical thickness, it means to 6–15 nm, allows for avoiding the creation of misfit dislocations. In such a layer, crystal lattice deforms elastically and adopts the substrate lattice. Its cells are biaxially compressed in the plane parallel to the $In_xGa_{1-x}As/InP$ boundary and uniaxially stretched in the crystal growth direction. It is a pseudomorphic, compressively strained layer. However, such a thin layer can absorb only about 1% of the radiation passing through it, thus the photodiode quantum efficiency is of the same order.

The solution providing improvement in the photodetector detectivity by decreasing the dark current, while maintaining the high sensitivity, is employing the structure with a resonant cavity, so-called, resonant cavity enhanced (RCE) photodetector. In this case, the layer absorbing the detected radiation is placed inside a Fabry-Perot cavity formed by two parallel Bragg mirrors integrated into the device structure. Due to the resonance enhancement of the optical energy within the cavity, the thickness of the absorbing layer can be significantly decreased. It makes it possible to fabricate a photodetector based on InP, taking advantage of its mature, reliable technology, and to introduce a thin, pseudomorphic $In_xGa_{1-x}As$ ($0.6 < x \le 0.83$) layer as the absorbing layer.

The concept of the RCE photodetection has appeared as a result of search of high-speed, high-efficiency photodetectors for optical communication [3,4]. The first RCE photodiodes, based on GaAs, have been optimised with respect to these features. Then, additional advantage of this type of photodiodes has been noticed [5], namely the reduction of the dark current compared to the conventional photodiode current. It has been observed in RCE photodiodes with a thin $In_{0.53}Ga_{0.47}As$ absorbing layer, lattice matched to the InP substrate. Afterwards the RCE

*e-mail: zynek-j@itme.edu.pl

photodiode with a thin, strained $In_{0.83}Ga_{0.17}As$ absorbing layer has been presented [6]. The decrease in the dark current density to 10^{-6} A/cm^2 has been caused both by the decrease in the thickness of layer in which mainly the generation current arises and by the decrease in the misfit dislocation density (in the concentration of thermal generation centres) in this layer. The photodiode detectivity at the room temperature has achieved 7×10^{11} cmHz$^{1/2}$/W.

In this paper, the results of the work aiming at development of a RCE photodiode operating at 1.9 μm are described. Such photodiodes should be especially useful for remote sensing, for cooperation with solid-state lasers with active dopant Tm^{3+} and Ho^{3+}. They can be applied in eye-safe rangefinding, lidar, moisture analysers, gas contamination monitoring, process control etc. An important application is the measurement of the moisture content in agricultural products by measuring water absorption at 1.9 μm.

2. Design considerations

The general structure of the RCE photodiode is presented in Fig. 1. It comprises a p-i-n junction (made of a non-absorbing, wider bandgap semiconductor) with a thin, undoped absorbing layer inserted into the depletion region. This junction is placed inside a resonant cavity formed by two parallel, distributed Bragg mirrors (DBR), consisting of quarter-wave alternating layers which are made of the materials capable of providing the desired refractive index contrast.

The photodiode performance depends on the properties of absorbing region, p-i-n junction, and resonant cavity. The spectral range of the detected radiation depends essentially on the employed absorption region. The dependence of the interband absorption cutoff wavelength on the indium content in a thick, unstrained $In_xGa_{1-x}As$ layer and in thin, strained $In_xGa_{1-x}As$ layers is shown in Fig. 2. It is assumed that the thin layer thickness equals the critical thickness. When $x < 0.6$, the decrease in the cutoff wavelength in the strained layer is caused mostly by changes of the band structure due to the strain. In the case when the

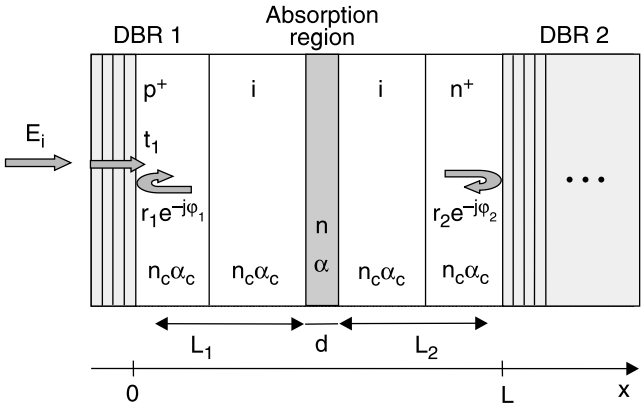

Fig. 1. General model of the RCE photodiode.

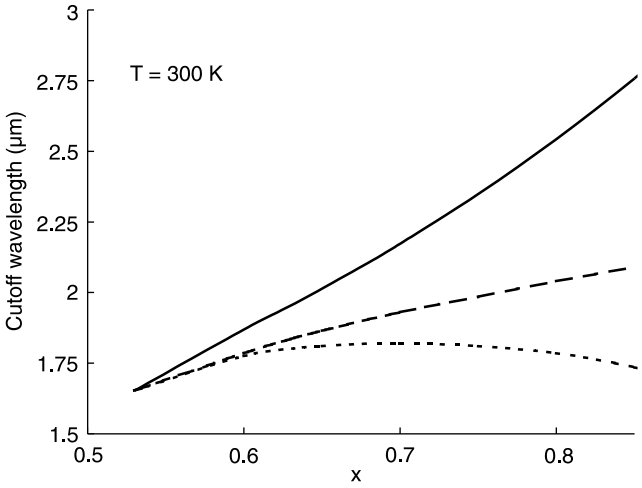

Fig. 2. Dependence of the interband absorption cutoff wavelength on the indium content in a thick, unstrained $In_xGa_{1-x}As$ layer (solid line) and in thin, strained $In_xGa_{1-x}As$ layers embedded between two InP layers (dotted line) or between two $In_{0.53}Ga_{0.47}As$ layers (dashed line). The thin layer thickness equals the critical thickness.

$In_xGa_{1-x}As$ layer with $x > 0.6$ is embedded between two layers with a wider bandgap, the size quantum effect causes the appearance of allowed energy levels in the conduction and valence bands. The energy of absorbed photons corresponds to the energy difference between the electron level in the conduction band and the heavy hole level in the valence band. When the In content increases, the strain in the pseudomorphic layer increases, the critical thickness decreases and the difference in cutoff wavelengths for thick, unstrained and thin, strained layer increases. In the case of the barrier made of InP, the cutoff wavelength does not attain 1.9 μm. The employment of the lower barrier made of $In_{0.53}Ga_{0.47}As$ enables us to shift the cutoff wavelength toward longer wavelengths.

The photodiode spectral response is strongly influenced by resonant cavity properties. They affect the spatial distribution of the optical field inside the cavity and the optical field enhancement. The part of the incident radiation, which is transmitted through the front mirror into the resonant cavity, is subject to multiple internal reflections at both mirrors as only a small fraction of this radiation is absorbed in the cavity at a single pass. The interference of two counter propagating waves forms the standing wave.

The electrical components of the electromagnetic field are considered since the electric field is the most important from the point of view of the interaction with a medium. The incident wave amplitude can be denoted as E_i. Every photodiode layer is characterised by the refractive index n, absorption coefficient α, and a thickness. The amplitude transmittance coefficient of the front mirror is denoted by t_1 and the amplitude reflection coefficients of the front and back mirrors are $r_1\exp(-j\varphi_1)$ and $r_2\exp(-j\varphi_2)$, respectively.

At $x = 0$, the wave propagating in the direction of the incident wave is the sum of the wave transmitted through the front mirror and the wave reflected at both mirrors

$$E^+(0) = t_1E_i + r_1r_2\exp[-\alpha d-\alpha_c(L_1 + L_2)] \exp[-j(2\beta L + \varphi_1 + \varphi_2)]E^+(0). \quad (1)$$

At $x = L$, the wave propagating in the direction opposite to the incident wave direction is

$$E^-(L) = r_2\exp[-\alpha d/2 - \alpha_c(L_1 + L_2)/2] \exp[-j(\beta L + \varphi_2)]E^+(0). \quad (2)$$

The total electric field in the cavity is the resultant of both waves

$$E(x) = E^+(0)\exp(-j\beta x) + E^-(L)\exp[j\beta(x - L)], \quad (3)$$

where $\beta = 2\pi n_c/\lambda_o$ is the propagation wave coefficient and λ_o is the wavelength in a free space. The photodiode quantum efficiency is related to the ratio $|E(x)|^2/|E_i|^2$ which determines the optical field power enhancement and can be derived from Eqs. (1), (2) and (3). The maximum enhancement of the field occurs when the wave reflected at both mirrors has the same phase as the incident wave

$$2\beta(\lambda_o)L + \varphi_1(\lambda_o) + \varphi_2(\lambda_o) = 2\pi m \ (m = 1,2,3....). \quad (4)$$

The coefficients β, φ_1, φ_2, as well as t_1, r_1, r_2, depend strongly on the wavelength. The variation of the reflection coefficients and particularly their phases with wavelength has significant influence on the quantum efficiency spectrum. The resonant nature of these effects causes confinement of the photoresponse spectra.

The quantum efficiency attains its maximum value when the back mirror power reflectivity approaches unity ($R_2 = r_2^2 \approx 1$) and the front mirror reflectivity is

$$R_1 = r_1^2 = R_2\exp(-2\alpha d). \quad (5)$$

The transmittance and reflection coefficients of mirrors can be computed by the transmission matrix method commonly used for the electromagnetic field analysis in the multilayer structures. Each layer can be represented by a 2×2 transmission matrix which establishes the relationships between the field components at the layer boundaries. When the reflectivity of a stack of layers is computed, the corresponding matrices are multiplied from the bottom to the top.

The transmission matrix method enables us to compute directly the reflectivity spectrum of the whole photodiode structure considering the resonant cavity as an assembly of layers characterised by their transmission matrices [7].

A photodiode structure has been designed assuming that the resonant cavity is made of InP, the back mirror consists of $In_{0.53}Ga_{0.47}As$/InP quarter-wave layers which are transparent for the wavelengths longer than 1.7 μm, and the front mirror is composed of SiO_2/Si quarter-wave layers. Twenty pairs of $In_{0.53}Ga_{0.47}As$/InP layers are required for the power reflectivity near unity. The phase shift at the maximum reflectivity is $\varphi_2 = \pi$. The front mirror has been designed considering Eq. (5). When the absorption coefficient in $In_xGa_{1-x}As$ is $\alpha \geq 10^4$ cm^{-1}, the $In_xGa_{1-x}As$ layer thickness is about 10 nm and the absorption coefficient in InP is α_c <10 cm^{-1}, two pairs of SiO_2/Si layers are necessary to achieve the maximum quantum efficiency. In this case, the power reflectivity attains $R_1 = 0.96$ and the phase shift at the maximum reflectivity is $\varphi_1 = 0$. The calculation of the optical field power enhancement factor $|E(x)|^2/|E_i|^2$ needs the knowledge of the exact value of the coefficient αd, however, this factor exceeds 40. When a single pair of SiO_2/Si layers is used, the reflectivity is $R_1 = 0.8$ and the field enhancement factor is about 28. In this case, the spectral response is lower and wider than in the first case. Without a dielectric mirror the native mirror exists at the air/InP interface providing the reflectivity $R_1 = 0.3$ sufficient to give the field enhancement factor equal to 6.5.

The distribution of the standing wave power in the designed structure is shown in Fig. 3. Considering the resonant condition (4), the parameter $m = 5$ has been chosen. The length of the cavity should be sufficient to fit the p-i-n junction with good electrical parameters into this cavity. The absorbing layer can be more accurately located at the standing wave maximum when it is placed near the back mirror. The dependence of the optical field power enhancement on αd for a large range of its values is presented in Fig. 4. The field enhancement increases with decreasing cavity losses (when αd decreases and the reflectivities R_1, R_2 increase).

3. Experimental results

The schematic structure of the designed RCE photodiode is shown in Fig. 5(a). The bottom mirror consisting of n-type $In_{0.53}Ga_{0.47}As$ and InP alternating layers, the resonant cavity composed of layers InP/$In_{0.53}Ga_{0.47}As$/$In_xGa_{1-x}As$/$In_{0.53}Ga_{0.47}As$/InP and the top p^+- type $In_{0.53}Ga_{0.47}As$ contact layer have been grown on the S-doped InP substrate by MOCVD. Twenty $In_{0.53}Ga_{0.47}As$/InP layer pairs, forming the bottom mirror, have been very well lattice matched to the substrate in order to avoid creation of misfit disloca-

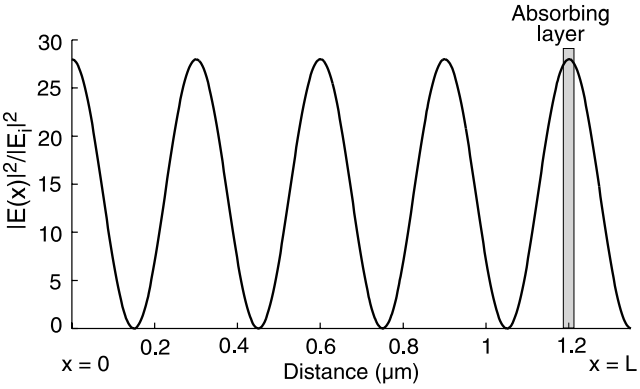

Fig. 3. Optical field power distribution in the resonant cavity of the designed RCE photodiode at $\lambda = 1.9$ μm.

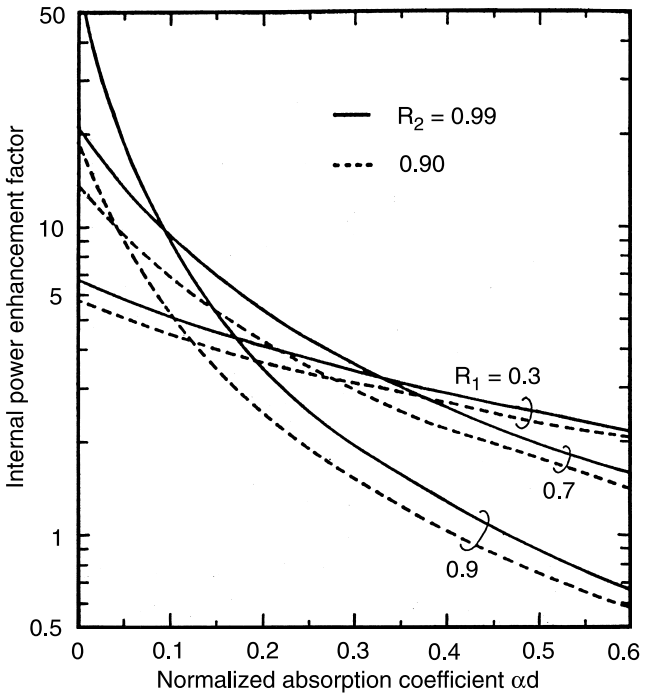

Fig. 4. Power enhancement factor in resonant cavities with various end mirror reflectivities as a function of the normalised absorption coefficient (after Ref. 3).

tions. Growth conditions of the strained $In_xGa_{1-x}As$ layers ($0.65 \le x \le 0.8$) of thickness approaching the critical thickness have been investigated. The crystal structure has been examined by Nomarski microscope, X-ray diffraction and photoluminescence measurements. The $In_xGa_{1-x}As$ layer with $x \approx 0.75$ has been chosen as the absorbing layer. The p^+-i junction has been formed in undoped InP by the diffusion of zinc from the top InP and $In_{0.53}Ga_{0.47}As$ layers which have been maximally doped with Zn during the epitaxial growth. A very good reproducibility of Zn concentration profile has been obtained. A SEM image of the heterostructure cross-section can be seen in Fig. 5(b).

Ti/Pt/Au and AuGe/Ni/Au ohmic contacts have been sputtered onto the p^+ side and onto the n^+ side, respectively and have been RTA annealed. The top p^+ $In_{0.53}Ga_{0.47}As$ layer has been etched away in the photosensitive region and left in the contact region. The top mirror made of Si/SiO_2 layers has been deposited on the revealed InP layer by the sputtering method. Mesa structures have been defined by wet chemical etching.

Predispositions of the fabricated epitaxial heterostructures to the RCE detection at the wavelengths about 1.9 μm have been examined on wafers before processing using secondary ion mass spectroscopy (SIMS), photoluminescence (PL), and reflectivity spectra measurements. Figure 6 shows typical SIMS profiles of a fabricated heterostructure. Four pairs of $In_{0.53}Ga_{0.47}As$/InP layers of the bottom mirror, resonant cavity with the absorbing layer, contact $In_{0.53}Ga_{0.47}As$ layer, and Zn concentration profile can be distinguished. The PL spectrum of this structure can be seen in Fig. 7. This spectrum is compared to the PL spectrum of a structure without the resonant cavity (without the bottom mirror). The both heterostructures have been fabricated in a MOCVD reactor, one after another, and in both cases the p-i-n junctions and the strained layers have been grown under the same conditions. PL measurements have been made at the same time. The structure without the cavity has a wide PL spectrum with maximum at 1910 nm. The PL spectrum of the structure with the cavity has several peaks resulting from the resonant enhancement of the

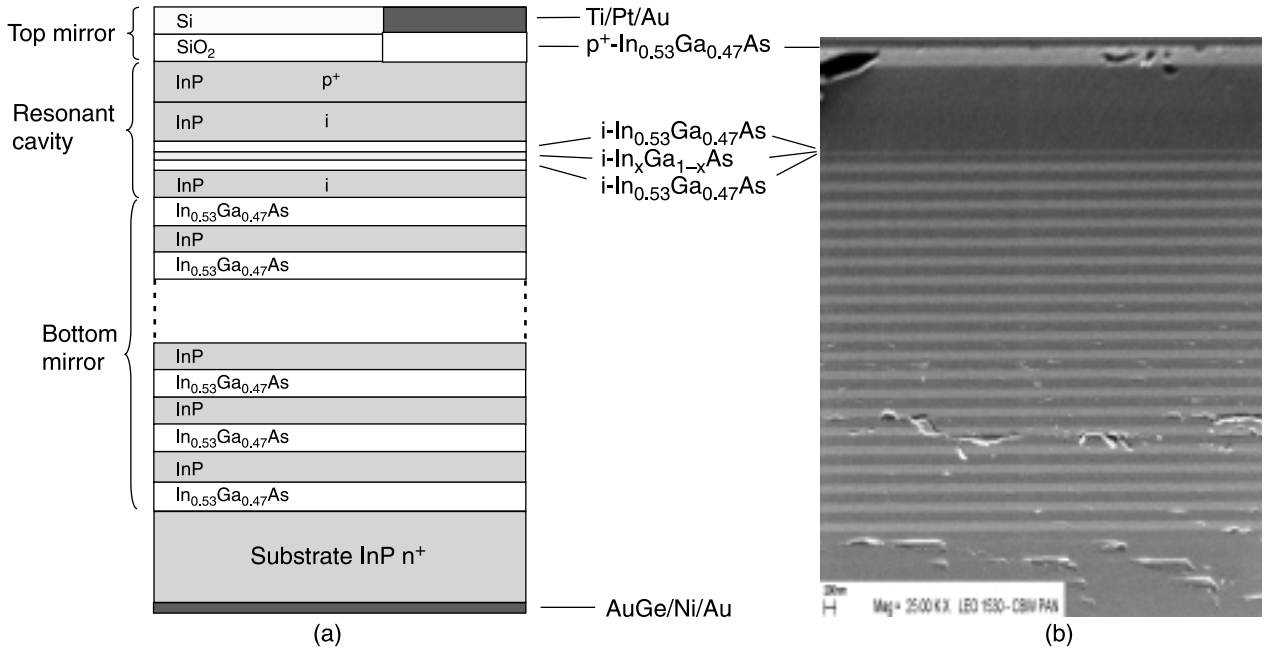

Fig. 5. Schematic structure of the designed RCE photodiode (a), SEM image of the cross-section of a RCE photodiode heterostructure grown by MOCVD (b).

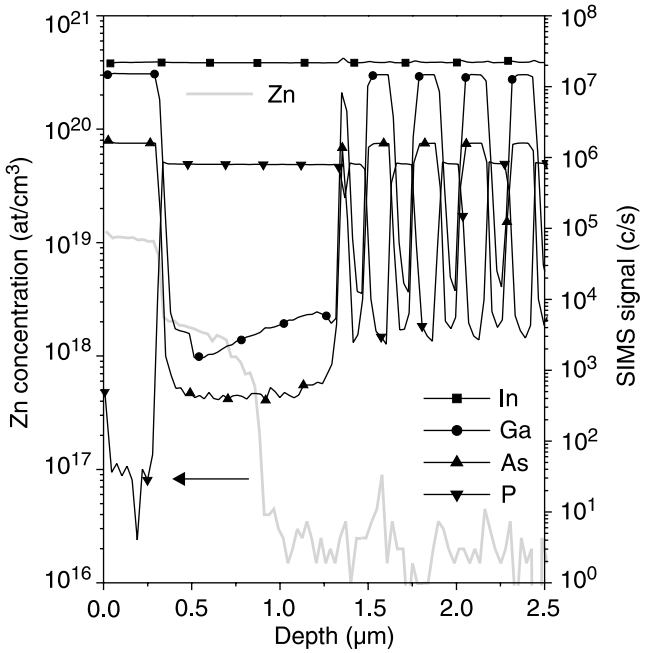

Fig. 6. Typical SIMS profiles of a RCE photodiode heterostructure grown by MOCVD.

PL signal for some wavelengths and the off-resonance decrease of this signal for other wavelengths. A high intensity of the PL signal at λ = 1900 nm (as for the native air/InP top mirror) gives evidence to an accurate location of the strained layer at the standing wave maximum. The power reflectivity spectrum of this structure is shown in Fig. 8. One can see the resonance at λ = 1900 nm at the Bragg mirror maximal reflectivity and the second resonance at λ = 1750 nm at the Bragg mirror minimal reflectivity. At

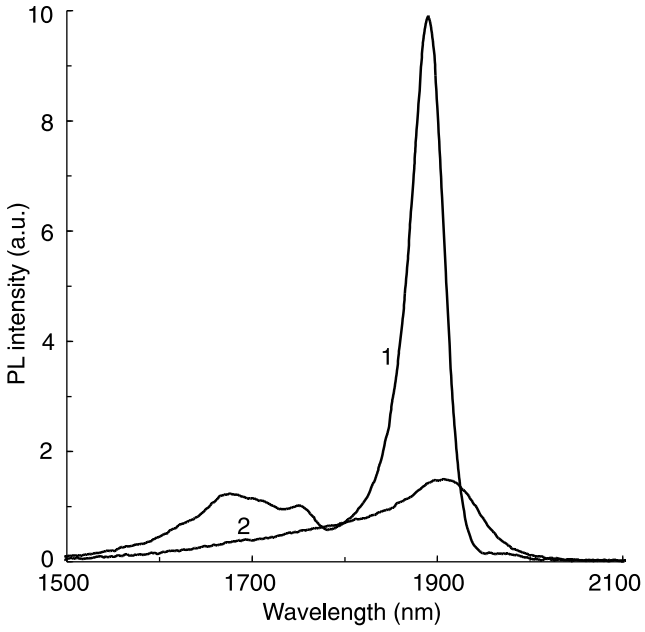

Fig. 7. PL spectra of photodiode heterostructures; with the cavity (1) and without the cavity (2).

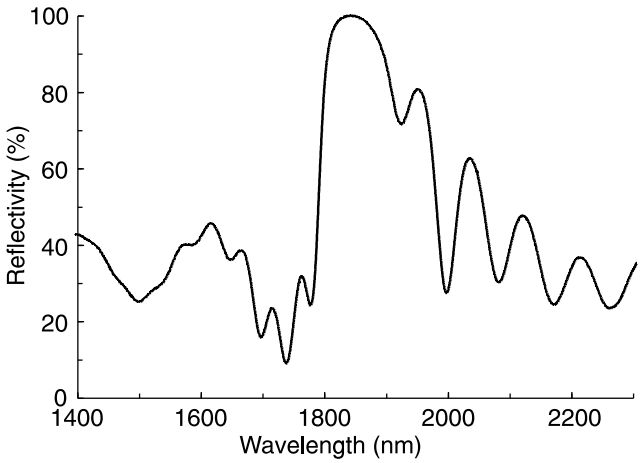

Fig. 8. Reflectivity spectrum of a fabricated RCE photodiode heterostructure.

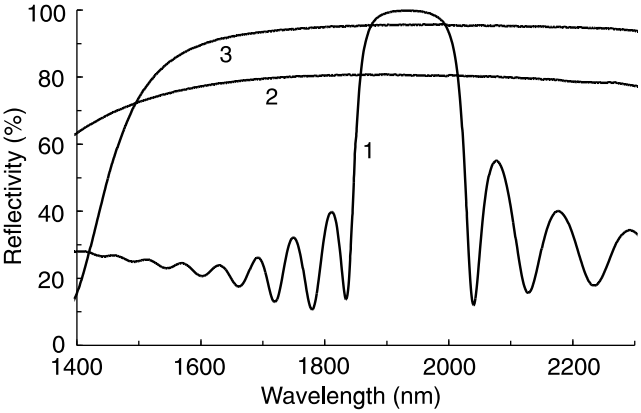

Fig. 9. Reflectivity spectra of Bragg mirrors; mirror composed of 20 pairs of $In_{0.53}Ga_{0.47}As/InP$ layers grown on the InP substrate (1), mirror composed of one pair of Si/SiO_2 layers sputtered on the InP substrate (2), and mirror composed of two pairs of Si/SiO_2 layers sputtered on the InP substrate (3).

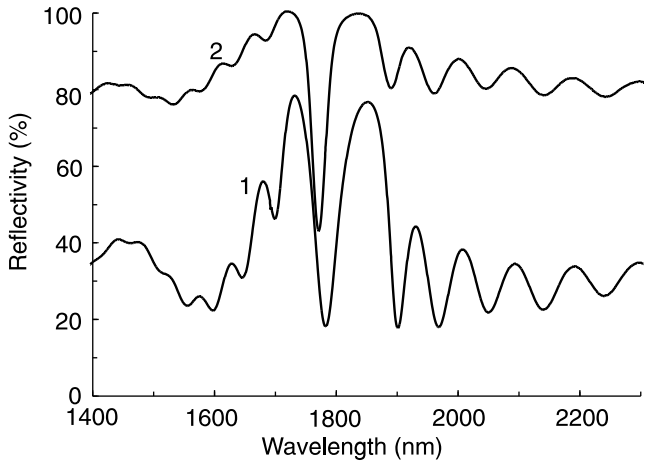

Fig. 10. Reflectivity spectra of a RCE photodiode heterostructure with the native air/InP top mirror (1) and after the deposition of a single pair of Si/SiO_2 layers as the top mirror (2).

the first resonance, a very high increase in the PL signal occurs, while the second resonance causes a very low PL intensity enhancement. The reflectivity spectrum of a bottom mirror deposited on a separate InP wafer, under the same conditions as the mirror of the complete structure, is shown in Fig. 9. The reflectivity spectra of another heterostructure with the cavity are presented in Fig. 10. One plot is related to the structure with the native air/InP top mirror and another one to this structure with a single pair of Si/SiO_2 layers deposited on its surface as a top mirror. The resonant fall of the reflectivity can be seen at the centre of the bottom mirror spectral characteristics. The reflectivity spectra of the top mirrors deposited on separate InP wafers under the same conditions as the mirrors of the complete structures are shown in Fig. 9. When PL and reflectivity spectra indicate that the resonance occurs at the wavelengths longer than 1900 nm, it is possible to tune the wavelength by recess etching. The reflectivity and PL spectra of an as-grown wafer and of the same wafer after etching away 70 nm of p^+ InP layer can be seen in Figs. 11 and 12, respectively. Especially the PL spectra differ significantly. After etching, the cavity resonance wavelength corresponds to the wavelength of the maximum of the PL spectrum measured for the structure without the cavity (Fig. 7). The decrease in the reflectivity after etching is caused by the deterioration of the surface quality after etching.

Typical reverse current-voltage characteristics of the fabricated photodiodes are shown in Fig. 13. The dark current density of a complete RCE photodiode (with the p-i-n junction grown on the $In_{0.53}Ga_{0.47}As$/InP layer stack) slightly exceeds 10^{-6} A/cm^2 at $U = -1$ V. When the same p-i-n junction is grown directly on the InP substrate, the dark current density is two times lower. Experiments of replacing a single strained $In_{0.75}Ga_{0.25}As$ layer by two such layers separated by an $In_{0.53}Ga_{0.47}As$ layer have been successfully made. Photodiodes without mirrors and with two strained layers inserted into the depletion region exhibit the

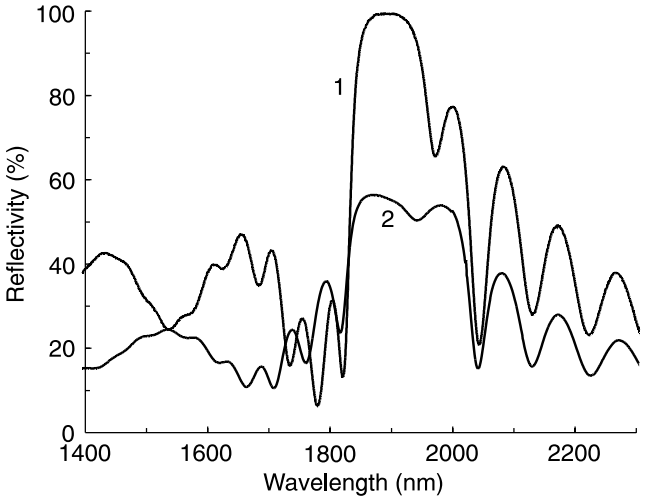

Fig. 11. Reflectivity spectra of a RCE photodiode heterostructure measured on as-grown wafer (1) and on the same wafer after recess etching (2).

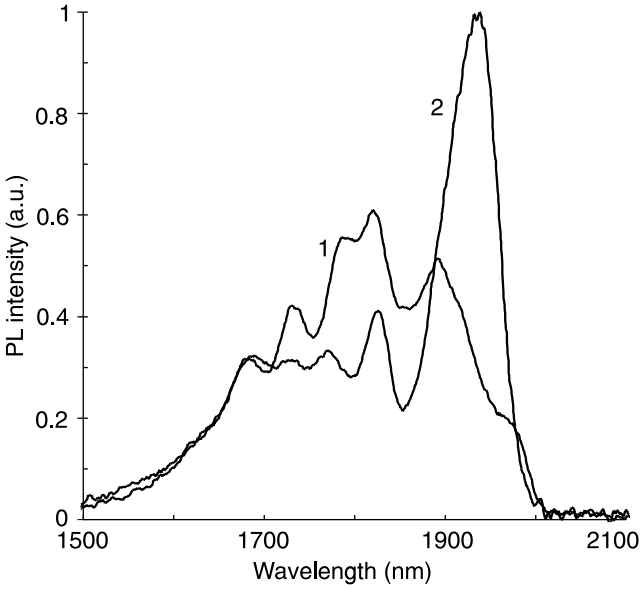

Fig. 12. PL spectra of a RCE photodiode heterostructure measured on as-grown wafer (1) and on the same wafer after recess etching (2).

dark current two times higher at $U = -5$ V than similar photodiodes with one strained layer. Since the quantum efficiency increases in this case, it is supposed that the employment of the two absorbing layers in the designed RCE photodiode should improve the detectivity. The contribution of individual layers of the p-i-n junction to the total dark current has been investigated. The dark current density of the p-i-n junction made of InP is typically about 10^{-9} A/cm^2. When a 20-nm thick $In_{0.53}Ga_{0.47}As$ layer is inserted into the InP depletion region, the dark current density of 10^{-7} A/cm^2 is measured. All the currents result from thermal generation of carriers and increase very slowly with a voltage. Since the generation currents in InP and $In_{0.53}Ga_{0.47}As$ layers are significantly lower than the cur-

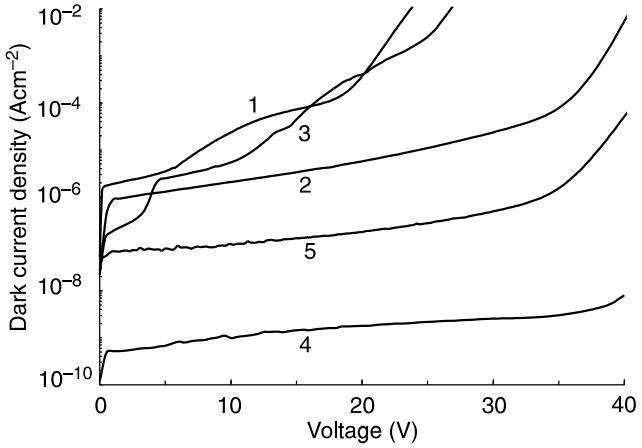

Fig. 13. Typical dark current density vs. reverse voltage characteristics of fabricated photodiodes; complete RCE photodiode (1), without the bottom mirror with a single absorbing layer (2), without the bottom mirror with two absorbing layers (3), p-i-n junction made of InP (4), p-i-n junction made of InP with a thin (20 nm) $In_{0.53}Ga_{0.47}As$ layer inserted into the depletion region (5).

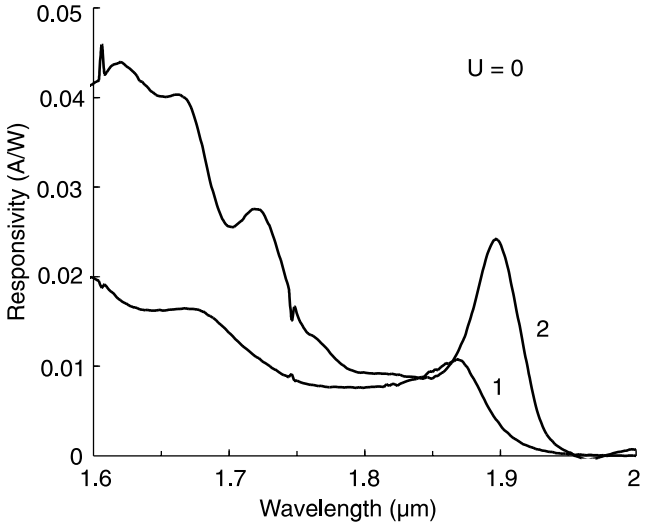

Fig. 14. Spectral response of photodiodes with a strained $In_{0.75}Ga_{0.25}As$ absorbing layer: photodiode without the resonant cavity (1), complete RCE photodiode with native air/InP top mirror (2).

rent in the strained layer, the photodiode current arises in practice in the strained layer.

The spectral responses of a photodiode without the cavity and with the cavity, when the top mirror is the native air/InP interface, are presented in Fig. 14. This is a preliminary result demonstrating the effect of the resonant enhancement of the responsivity. The enhancement factor is 2.3 instead of 6.5 predicted for the designed RCE photodiode with the native air/InP top mirror. The recess etching of the photosensitive surface and the deposition of the top mirror should improve the responsivity.

4. Conclusions

The technology of the RCE photodiode operating at the wavelengths about 1.9 μm has been developed. Good quality of the pseudomorphic, strained $In_{0.75}Ga_{0.25}As$ layer surrounded by $In_{0.53}Ga_{0.47}As$/InP barriers ensures low level of thermal generation of carriers and sufficiently high level of photogeneration of carriers at the design wavelength. The dark current density of 10^{-6} A/cm^2 and the quantum efficiency of 0.8% at U = –1 V have been measured typically for photodiodes without the resonant cavity. Since the RCE performance of this photodiode depends on accurate realisation of the design, special care has been taken to characteriz the wafers before processing and, if necessary, adjust the resonant wavelength to the design wavelength. Since the replacement of a single strained $In_{0.75}Ga_{0.25}As$ layer by two such layers does not change significantly the dark current vs. voltage characteristics, it is a promising way to increase photodiode detectivity.

Acknowledgment

This work was partially supported by the Polish State Committee for Scientific Research (project no. 7T11B04120).

References

1. A.M. Joshi, G.H. Olsen, S. Mason, M.J. Lange, and V.S. Ban, "Near-infrared (1–3 μm) InGaAs detectors and arrays: crystal growth, leakage current and reliability", *Proc. SPIE* **1715**, 585–593 (1992).
2. Sensors Unlimited, Hamamatsu and XenICs product catalogues.
3. K. Kishino, M.S. Ünlü, J.I. Chyi, J. Reed, L. Arsenault, and H. Morkoç, "Resonant cavity-enhanced (RCE) photodetectors", *IEEE J. Quantum Electron.* **27**, 2025–2034 (1991).
4. M.S. Ünlü and S. Strite, "Resonant cavity enhanced photonic devices", *J. Appl. Phys.* **78**, 607–639 (1995).
5. B.N. Sverdlov, A.E. Botchkarev, N. Teraguchi, A.A. Salvador, and H. Morkoç, "Reduction of dark current in photodiodes by the use of a resonant cavity", *Electron. Lett.* **29**, 1019–1021 (1993).
6. S. Jourba, M.P. Besland, M. Gendry, M. Garrigues, J.L. Leclercq, P. Rojo-Romeo, P. Viktorovich, S. Cortial, X. Hugon, and C. Pautet, "2-μm resonant cavity enhanced InP/InGaAs single quantum well photo-detector", *Electron. Lett.* **35**, 1272–1274 (1999).
7. J.A. Jervase and H. Bourdoucen, "Design of resonant-cavity-enhanced photodetectors using genetic algorithms", *IEEE J. Quantum Electron.* **36**, 325–332 (2000).

Thanks to its little LABCam, ELDIM makes photometry and quantitative imaging affordable!

CMOS image sensors have for a long time been limited to the lower ranks of imaging applications, leaving the costly CCD systems the lion's share of the high performance market. Economics and the emergence of high-volume markets for high-grade CMOS sensors have changed this. To continue its position as a leading developer of high-grade imaging tools, ELDIM has developed a scientific-grade CMOS sensor based, low-cost digital camera. LABCam provides a true alternative to CCD systems for industrial imaging and optical metrology applications.

Compact and low power, the **LABCam** reduces costs without sacrificing image quality. Its one mega-pixel resolution, rapid data acquisition and wide measurement range, make LABCam the ideal instrument for all types of quantitative imaging measurements: evaluation of screen uniformity, product quality control, medical and microscopic imaging.

Using CMOS imaging technology, **LABCam** allows individual pixel addressing via a dedicated processor. The user can easily control sensor saturation and exposure and zoom on a region of interest while acquiring samples or full images.

LABCam's 10-bit per pixel sensor provides rapid acquisition while the USB 2.0 interface speeds data transfer rates to 480 Mbits/s through a simple standard interface. **LABCam** comes complete with camera control and data processing software. Advanced users can easily modify the software's functions using the development kit provided (examples of code are supplied).

An optional photopic filter allows photometric measurements and, for applications requiring increased low-level sensitibity, an cooled sensor version is available. ELDIM rounds out their imaging product line with the iSENSE and MURATest cameras, both of which utilize cooled, scientific-grade CCD sensors for superior performance.

ELDIM is looking for distributors to promote its range of **LABCam** cameras locally.

In 2004, ELDIM will be participating at the trade shows:
Japan - FDP International, SEMI FPD Expo 2004, SID 2004, FINETECH 2004; Taiwan – DISPLAY Taiwan, SEMICON Taiwan; Korea – LED Expo, ASID 2004; China – OPTO China

For more information, please contact:

Société ELDIM
Mr Luc MARGERIE
Communication Manager
1185 rue d'Epron
14200 HEROUVILLE SAINT CLAIR
Tel: +33 (0) 2 31 94 76 00
Fax: +33 (0) 2 31 94 09 50
Email: eldim@eldim.fr
Website: www.eldim.fr

